

Supporting information

Sensitivity of tree species performance to climate and competition
changes across their range distribution

WILLIAN VIEIRA, ANDREW MACDONALD, DOMINIQUE GRAVEL

Contents

1 Supplementary Material 1	2
1.1 Model fit	2
1.2 Model comparison	2
1.3 Parameter variance	3
1.4 Model predictive accuracy	3
1.5 Leave-one-out cross-validation	4
1.6 Size effect in survival	7
1.7 Conclusion	9
2 Supplementary Material 2	10
3 Supplementary Mateiral 3	23
3.1 Sensitivity analysis	23
3.2 Simulation Summary	24
3.3 Importance of demographic models	24
3.4 Importance of covariates	28
3.5 Notes on Conspecific and Heterospecific Competition Effects	28
References	29

¹ **1 Supplementary Material 1**

² **1.1 Model fit**

³ We assessed the growth, survival, and recruitment rates by examining transitions between two
⁴ measurements. While we fitted the growth and survival functions at the individual level, recruitment
⁵ was evaluated at the plot level. Due to differences in measurement thresholds between the FIA and
⁶ Quebec protocols, we only considered individuals with a dbh ≥ 127 mm. Therefore, we quantified
⁷ the ingrowth rate as the number of individuals crossing the 127 mm threshold. We included trees
⁸ with at least two measurements over time to quantify growth and survival. Similarly, we used plots
⁹ with at least two measurements over time for ingrowth. To simplify the model hierarchy, we did not
¹⁰ incorporate temporal models. Instead, we treated two transition measurements for the same individual
¹¹ as independent information. The plot random effects partially accounted for the variation at the
¹² individual level, where different individuals with multiple measurements shared the same variation.

¹³ We fitted each of the growth, survival, and recruitment models separately for each species, using
¹⁴ the Hamiltonian Monte Carlo (HMC) algorithm via the Stan software (version 2.30.1 Team and
¹⁵ Others 2022) and the `cmdstanr` R package (version 0.5.3 Gabry et al. 2023). We conducted 2000
¹⁶ iterations for the warm-up and sampling phases for each of the four chains, resulting in 8000 posterior
¹⁷ samples. However, we kept only the last 1000 iterations of the sampling phase to save computation
¹⁸ time and storage space, resulting in 4000 posterior samples. We assessed model convergence using
¹⁹ Stan's \hat{R} statistic, considering convergence achieved when $\hat{R} < 1.05$. The complete code used for
²⁰ data preparation, model execution, and diagnostic analysis is hosted at <https://github.com/willyvieira/TreesDemography>. Diagnostic reports for all fitted models, including information on model
²¹ convergence, parameter distributions, prediction checks, R^2 , and other metrics, are available at
²² <https://willvieira.github.io/TreesDemography/>.

²⁴ **1.2 Model comparison**

²⁵ We constructed the demographic models incrementally, starting from the simple intercept model and
²⁶ gradually adding plot random effects, competition, and climate covariates. While the intercept-only
²⁷ model represents the most basic form, we opted to discard it and use the intercept model with
²⁸ random effects as the baseline or null model for comparison with more complex models. We ensured

29 the convergence of all these model forms, and comprehensive diagnostic details are available at
30 <https://github.com/willvieira/TreesDemography>.

31 Our primary objective is to select the model that has learned the most from the data. We used
32 complementary metrics to quantify the gain in information achieved by adding complexity to each
33 demographic model. One intuitive metric involves assessing the reduction in variance attributed to
34 likelihood and the variance associated with plot random effects. A greater reduction in their variance
35 implies a greater information gain from model complexity. The following metrics are all derived from
36 the idea of increasing predictive accuracy. Although we focus on inference, measuring predictive power
37 is crucial for quantifying the additional information gained from including new covariates. The first
38 two classic measures of predictive accuracy are the mean squared error (MSE) and the pseudo R^2 . We
39 base these metrics on the linear relationship between observed and predicted demographic outputs.
40 Finally, we used Leave-One-Out Cross-Validation (LOO-CV), which uses the sampled data to estimate
41 the model's out-of-sample predictive accuracy (Vehtari et al. 2017). LOO-CV allows us to assess how
42 well each model describes the observed data and compare competing models to determine which has
43 learned the most from the data.

44 1.3 Parameter variance

45 This section describes how the variance attributed to plot random effects changes with increasing
46 model complexity. As we introduce covariates, it is expected that part of the variance in demographic
47 rates, initially attributed to random effects, shifts towards the covariate fixed effects. Therefore, the
48 larger the reduction in variance associated with plot random effects, the more significant the role of
49 covariates in explaining demographic rates. The Figure 1 shows the σ_{plot} change with increased model
50 complexity for growth, survival, and recruitment vital rates.

51 1.4 Model predictive accuracy

52 We used pseudo R^2 and MSE metrics derived from comparing observed and predicted values to
53 evaluate the predictive accuracy of growth and recruitment demographic rates. Higher R^2 values and
54 lower MSE indicate better overall model accuracy. The Figures 2 and 3 compare the growth and
55 recruitment models using R^2 and MSE, respectively.

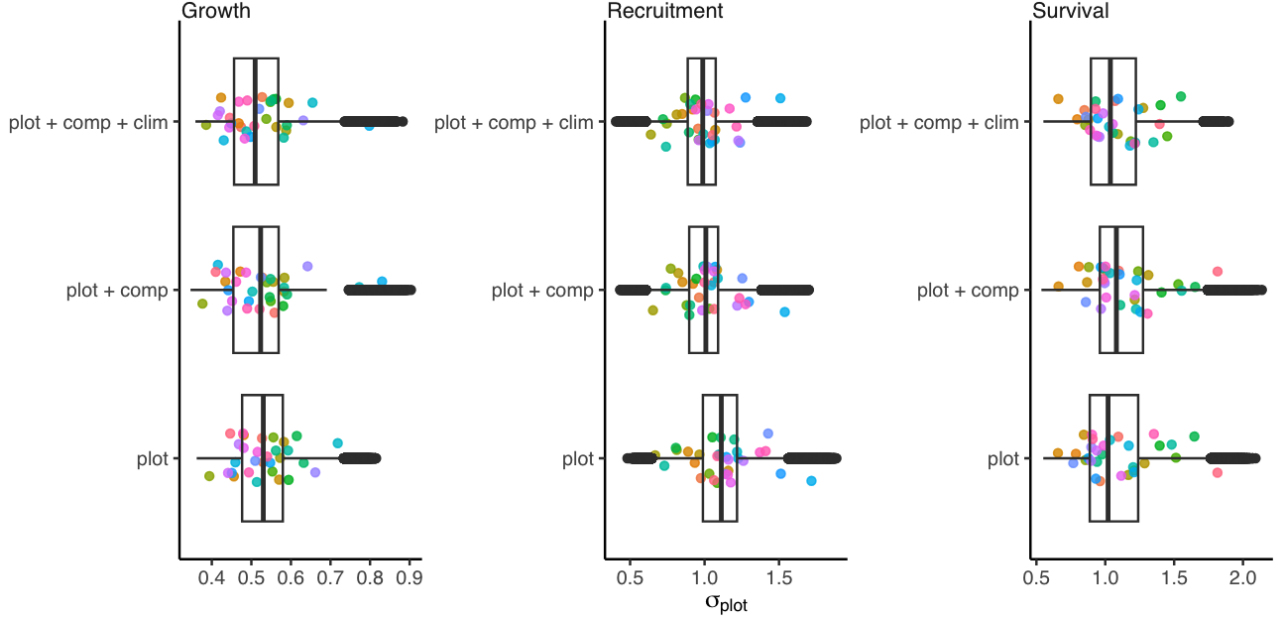


Figure 1: Boxplot showing the change in the posterior distribution of the parameter σ_{plot} across the 31 tree species between the competing models. For each growth, survival, and recruitment vital rate, the simplest model (plot random effects only) increases in complexity with the addition of fixed size, competition, and climate covariates. Each colored dot represents the species' average posterior distribution.

We used three complementary metrics for the survival model to assess model predictions. While the accuracy of classification models is often evaluated through the fraction of correct predictions, this measure can be misleading for unbalanced datasets such as mortality, where dead events are rare. To address this issue, we calculated sensitivity, which measures the percentage of dead trees correctly identified as dead (true positives). We also computed specificity, which measures the percentage of live trees correctly identified as alive (true negatives). The combination of sensitivity and specificity allows us to calculate corrected accuracy, considering the unbalanced accuracy predictions of positive and negative events (Figure 4).

1.5 Leave-one-out cross-validation

Finally, we evaluated the competing models using the LOO-CV metric (Figure 5), where models are compared based on the difference in the expected log pointwise predictive density (ELPD_diff). In cases involving multiple models, the difference is calculated relative to the model with highest ELPD (Vehtari et al. 2017). Consequently, the model with ELPD_diff equal to zero is defined as the best model. In contrast, the performance of the other models is assessed based on their deviation from

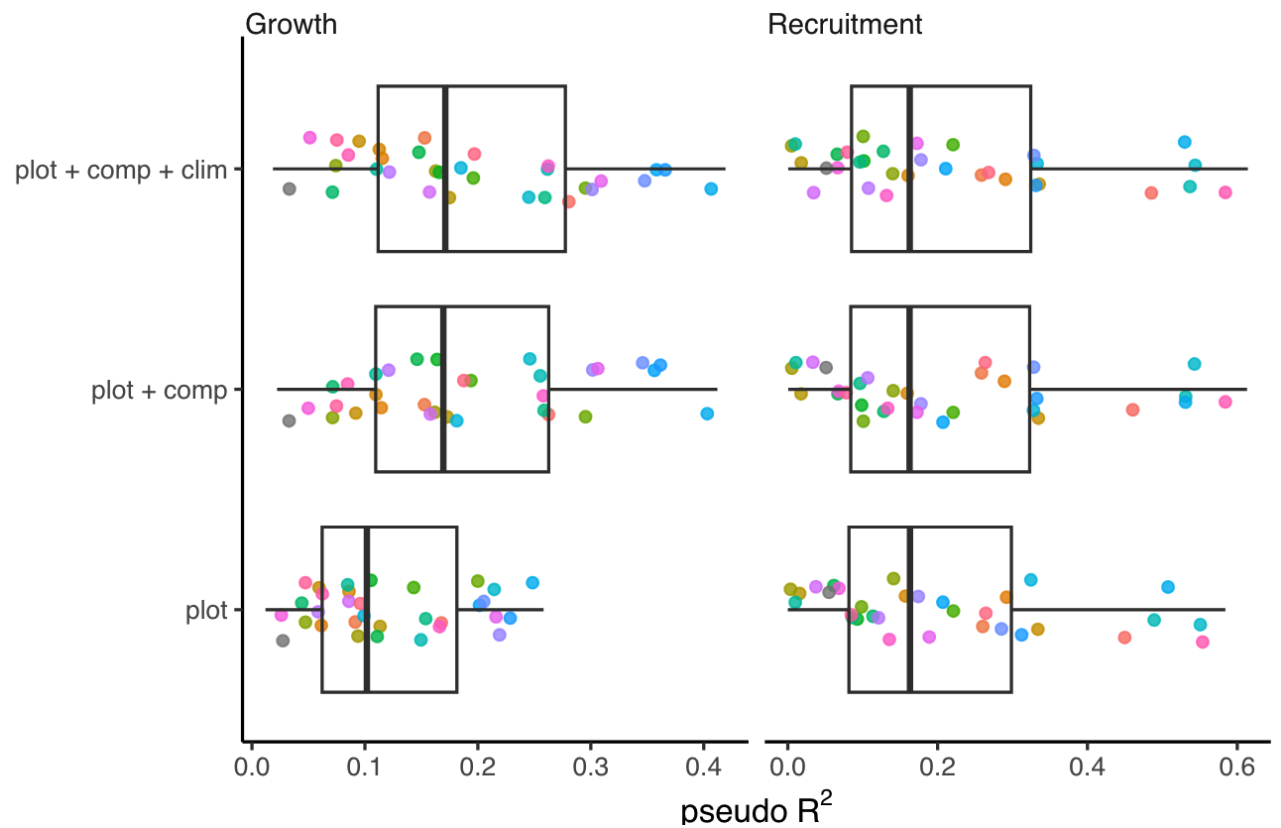


Figure 2: Posterior distribution of pseudo R^2 across the 31 tree species between the competing models. For each growth, survival, and recruitment vital rate, the simplest model (plot random effects only) increases in complexity with the addition of fixed competition and climate covariates. Each colored dot represents the species' average posterior distribution.

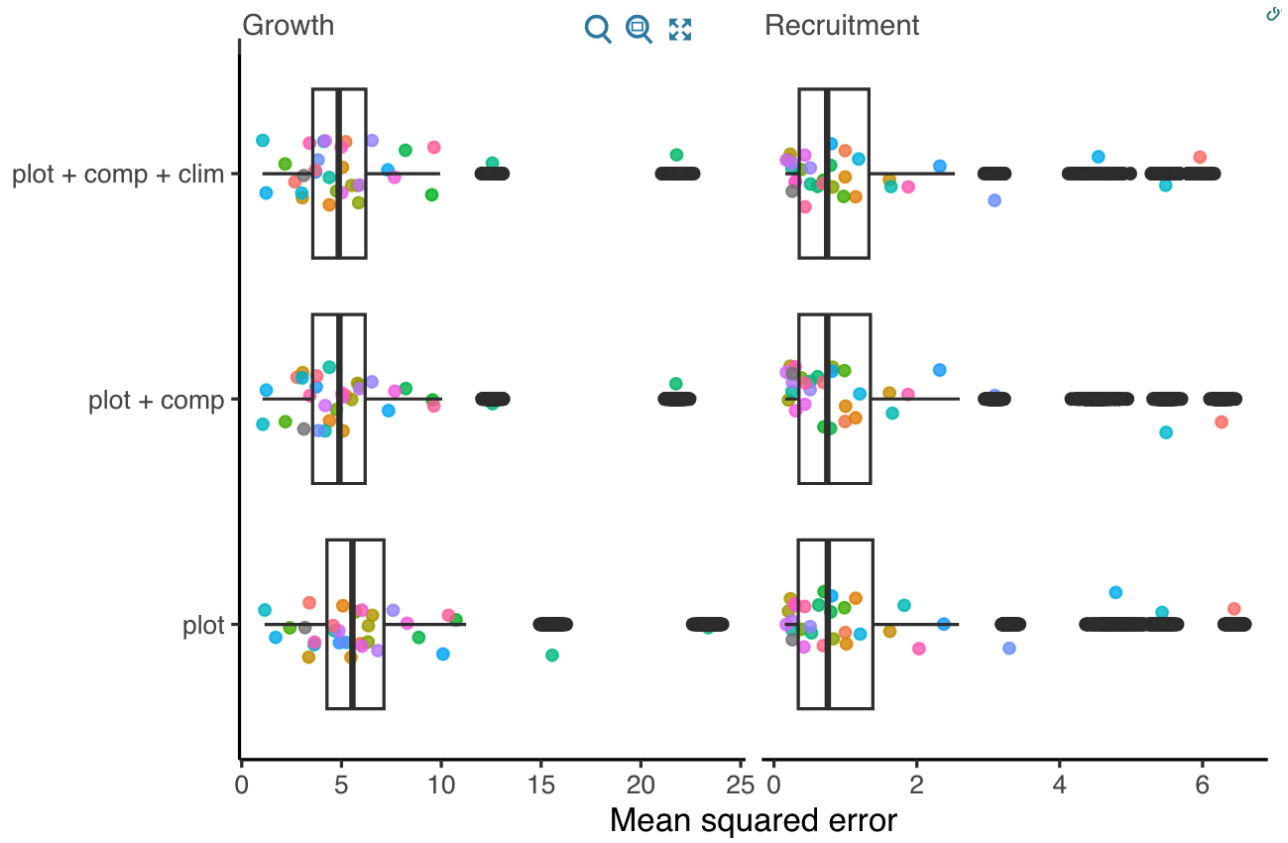


Figure 3: Posterior distribution of Mean Squared Error (MSE) across the 31 tree species as models become more complex.

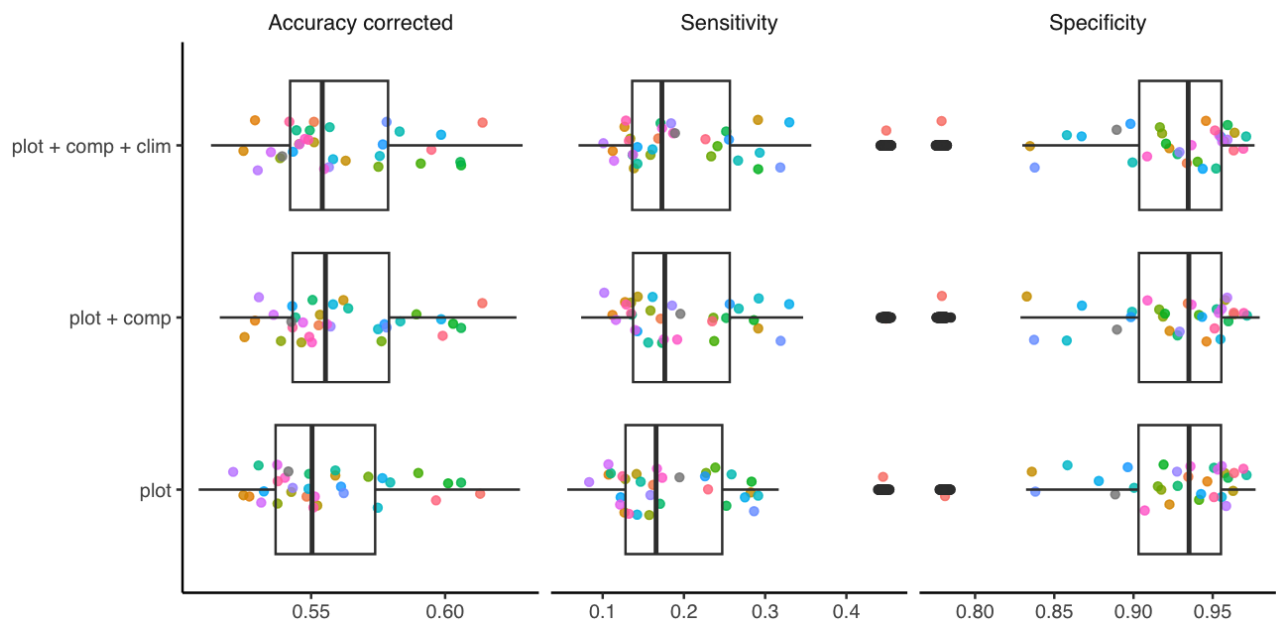


Figure 4: Comparing the posterior distribution of sensitivity, specificity, and accuracy across the 31 tree species between the competing models. Each colored dot represents the species' average posterior distribution.

70 the reference model in pointwise predictive cross-validation. Given the large number of observations
 71 in the dataset, we approximated LOO-CV using PSIS-LOO and subsampling. For each species, we
 72 approximated LOO-CV by sampling one-fifth of the total number of observations.

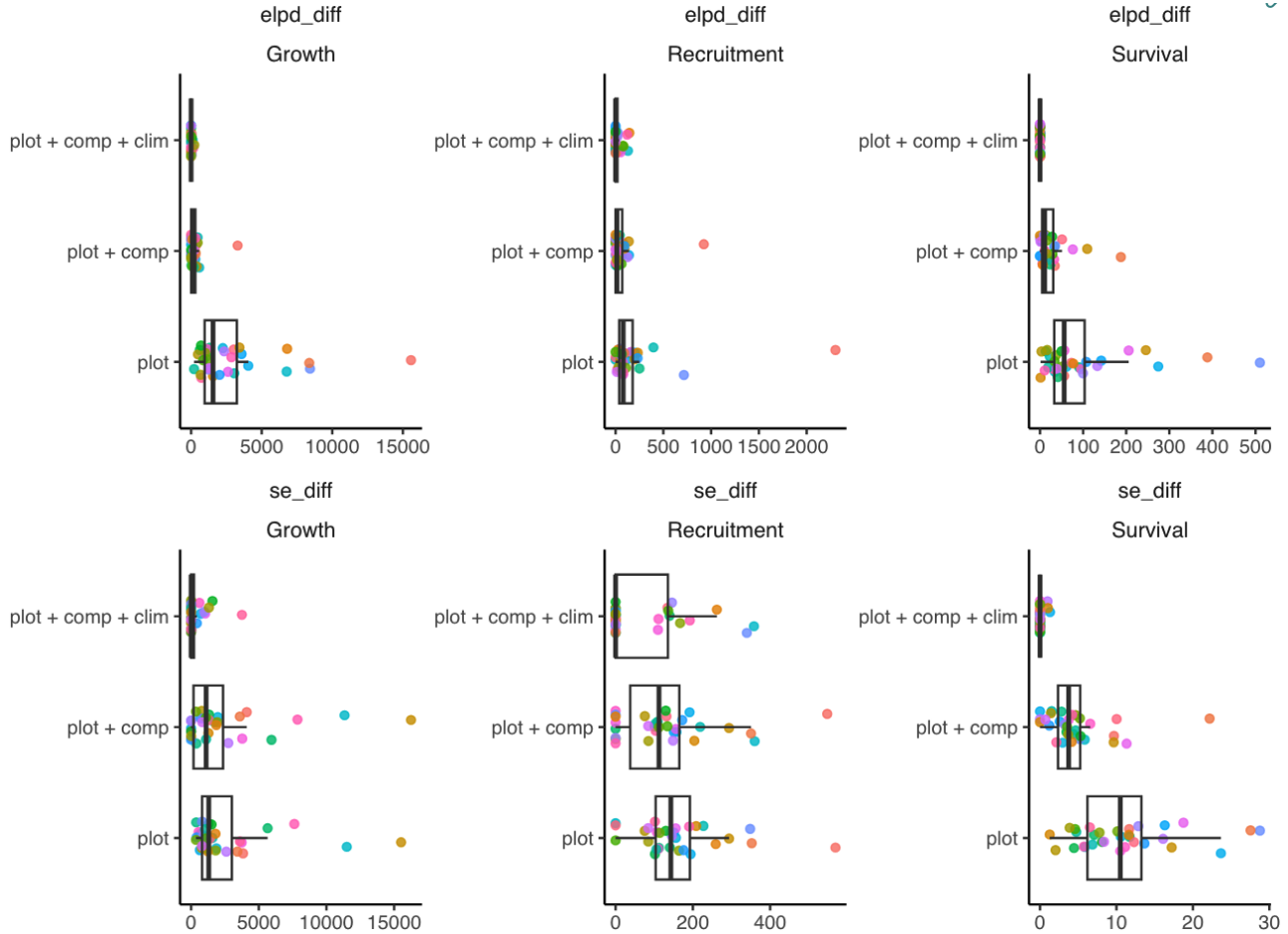


Figure 5: Boxplot shows the LOO-CV compare between the competing models based on the expected log pointwise predictive density (ELPD_diff) difference across the 31 tree species. The sd_diff is the standard error of the ELPD difference between the model and the reference model (ELPD_diff equal to zero).

73 1.6 Size effect in survival

74 We initially incorporated the size effect into the survival models due to the structured-population
 75 approach. However, we observed that the effect of size on mortality probability was generally weak and
 76 variable among species, with no clear pattern of increased mortality probability with larger individual
 77 size. All models that included the size effect performed worse than the null model, which contained
 78 only plot random effects (Figure 6).

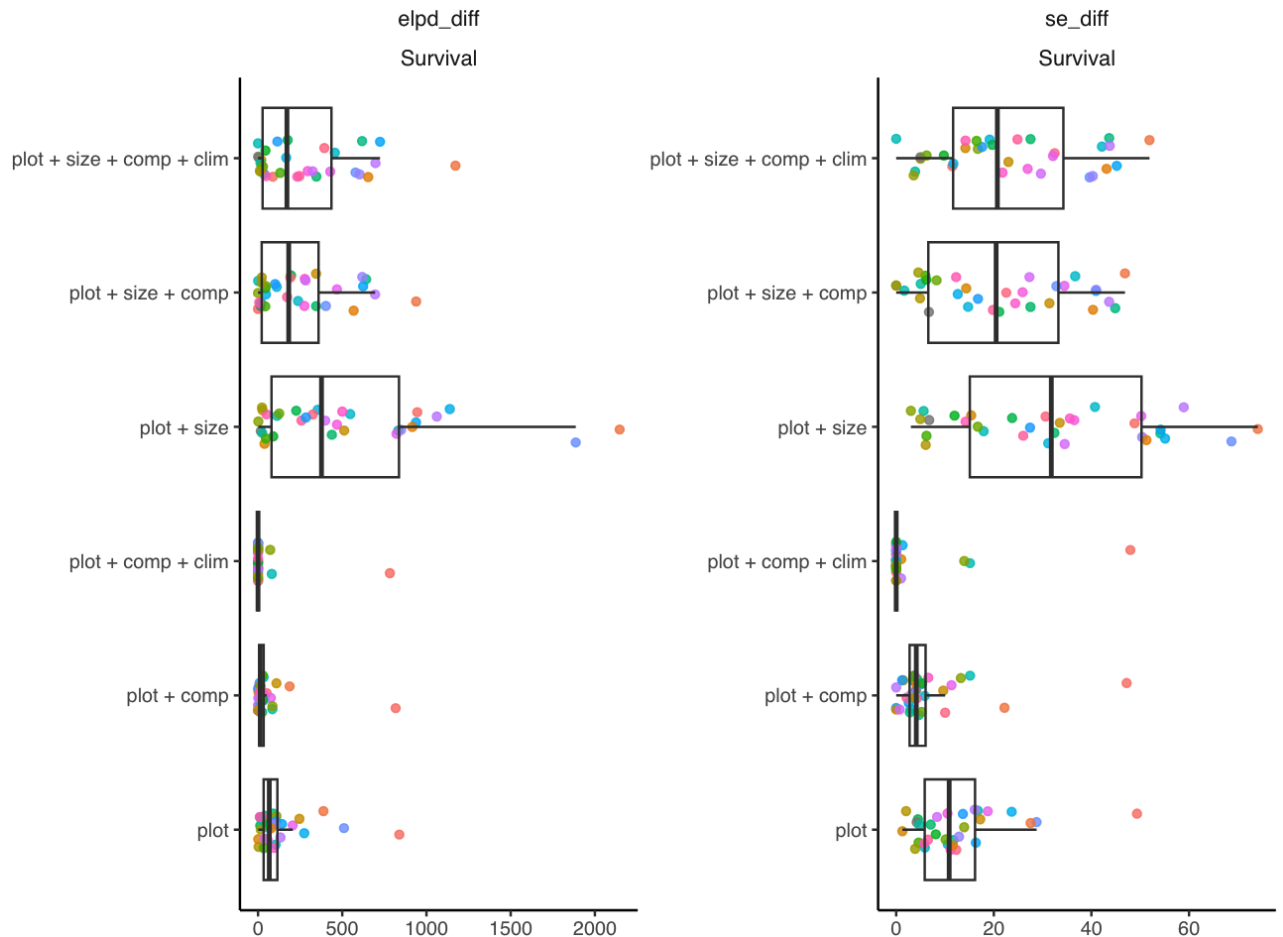


Figure 6: Boxplot shows the LOO-CV compare between the competing models based on the expected log pointwise predictive density (ELPD_diff) difference across the 31 tree species. The sd_diff is the standard error of the ELPD difference between the model and the reference model (ELPD_diff equal to zero).

79 **1.7 Conclusion**

80 Our analysis revealed that incorporating competition into the growth, survival, and recruitment models
81 proved more effective in gaining individual-level information than climate variables. The parameter
82 σ_{plot} , interpreted as spatial heterogeneity, was lowest in the growth model, followed by recruitment and
83 survival. As the models became more complex with the inclusion of covariates, recruitment exhibited
84 the most significant reduction in spatial variance, followed by growth, with no clear pattern in the
85 case of survival.

86 Regarding predictive performance, competition contributed more to the overall predictive capacity
87 (R^2 , MSE, and corrected accuracy) in the growth and survival models compared to climate variables.
88 Although recruitment had the largest reduction in σ_{plot} , it had minimal impact on prediction accuracy.

89 Finally, the LOO-CV indicates a clear trend where the complete model featuring plot random effects,
90 competition, and climate covariates outperformed the other competing models. Furthermore, the
91 absolute value of the ELPD shows that the growth model gained the most information from including
92 covariates, followed by recruitment and survival models. Consequently, we selected the complete
93 model with plot random effects, competition, and climate covariates as the preferred model for further
94 analysis.

95 2 Supplementary Material 2

Table 1: List of species and their frequency across the dataset.

Species	Number of plots	Number of individual	Number of observation
<i>Acer rubrum</i>	13149	96739	235408
<i>Abies balsamea</i>	11932	247737	521565
<i>Betula papyrifera</i>	9508	78049	203500
<i>Picea mariana</i>	7869	186491	454246
<i>Acer saccharum</i>	7403	71961	184641
<i>Picea glauca</i>	5889	27641	65626
<i>Populus tremuloides</i>	5876	56010	127115
<i>Betula alleghaniensis</i>	5624	28872	73116
<i>Quercus rubra</i>	4549	18272	46341
<i>Quercus alba</i>	4200	20376	51466
<i>Fagus grandifolia</i>	3819	21784	51764
<i>Prunus serotina</i>	3730	12178	26464
<i>Thuja occidentalis</i>	3230	51312	125811
<i>Pinus strobus</i>	3165	15638	38470
<i>Fraxinus americana</i>	2885	8942	21501
<i>Quercus velutina</i>	2722	10068	23298
<i>Tsuga canadensis</i>	2604	17914	45198
<i>Nyssa sylvatica</i>	2436	6275	15785
<i>Quercus stellata</i>	2279	14707	32102
<i>Picea rubens</i>	2190	16580	41674
<i>Liquidambar styraciflua</i>	2154	11655	29671
<i>Fraxinus pennsylvanica</i>	2149	9048	20588
<i>Tilia americana</i>	2059	8415	21412
<i>Pinus banksiana</i>	2057	34122	75372
<i>Populus grandidentata</i>	2015	13759	29358
<i>Fraxinus nigra</i>	1951	12633	31156

<i>Liriodendron tulipifera</i>	1912	8580	21071
<i>Carya tomentosa</i>	1636	3897	10590
<i>Carya glabra</i>	1622	4002	9916
<i>Quercus prinus</i>	1590	11000	27554
<i>Juniperus virginiana</i>	1571	9474	21400

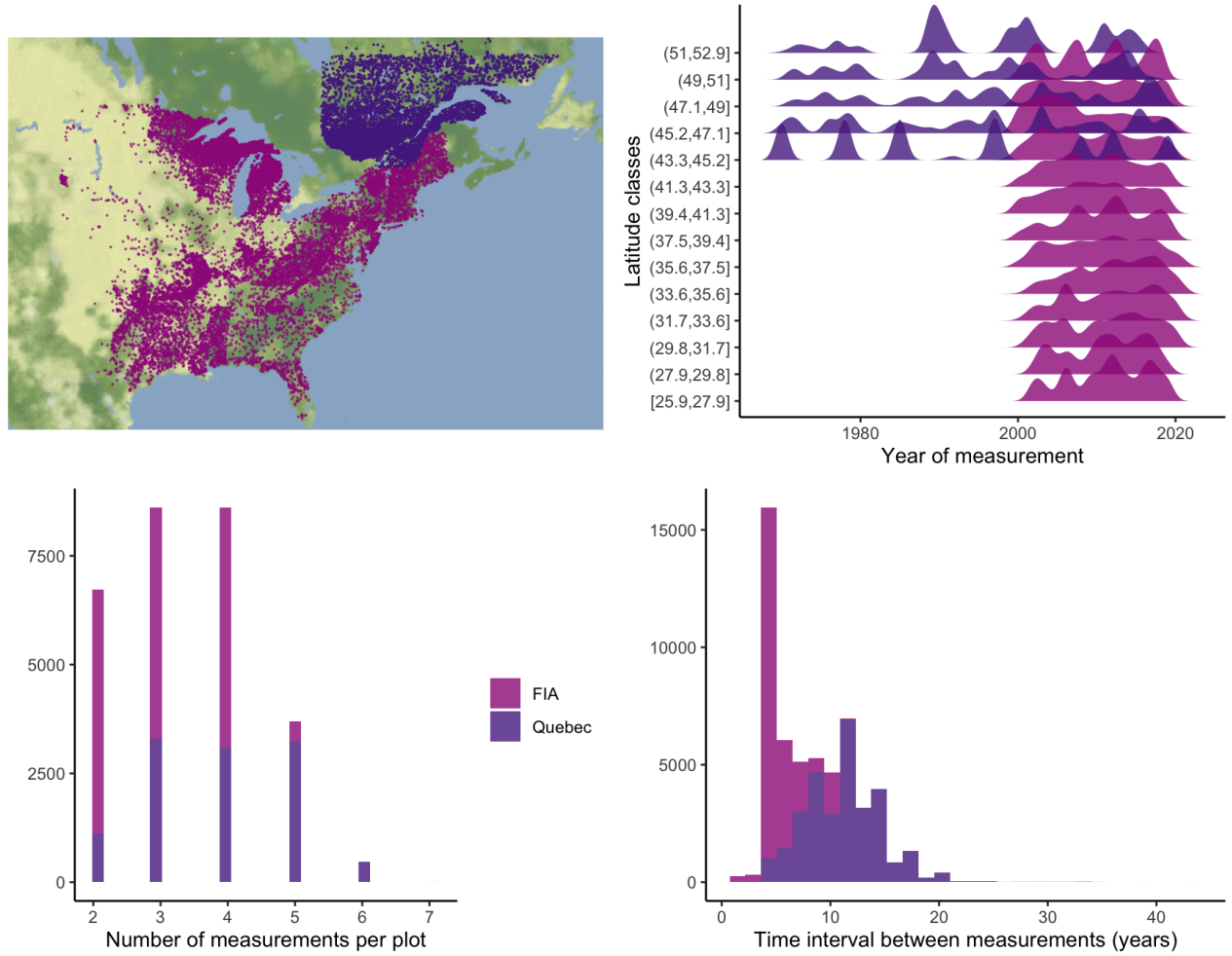


Figure 7: Spatial (top left) and temporal (top right) coverage of the dataset incorporating data from the USA and Quebec. The top right panel shows the distribution of observations per class of latitude for the 31 species used in this study.

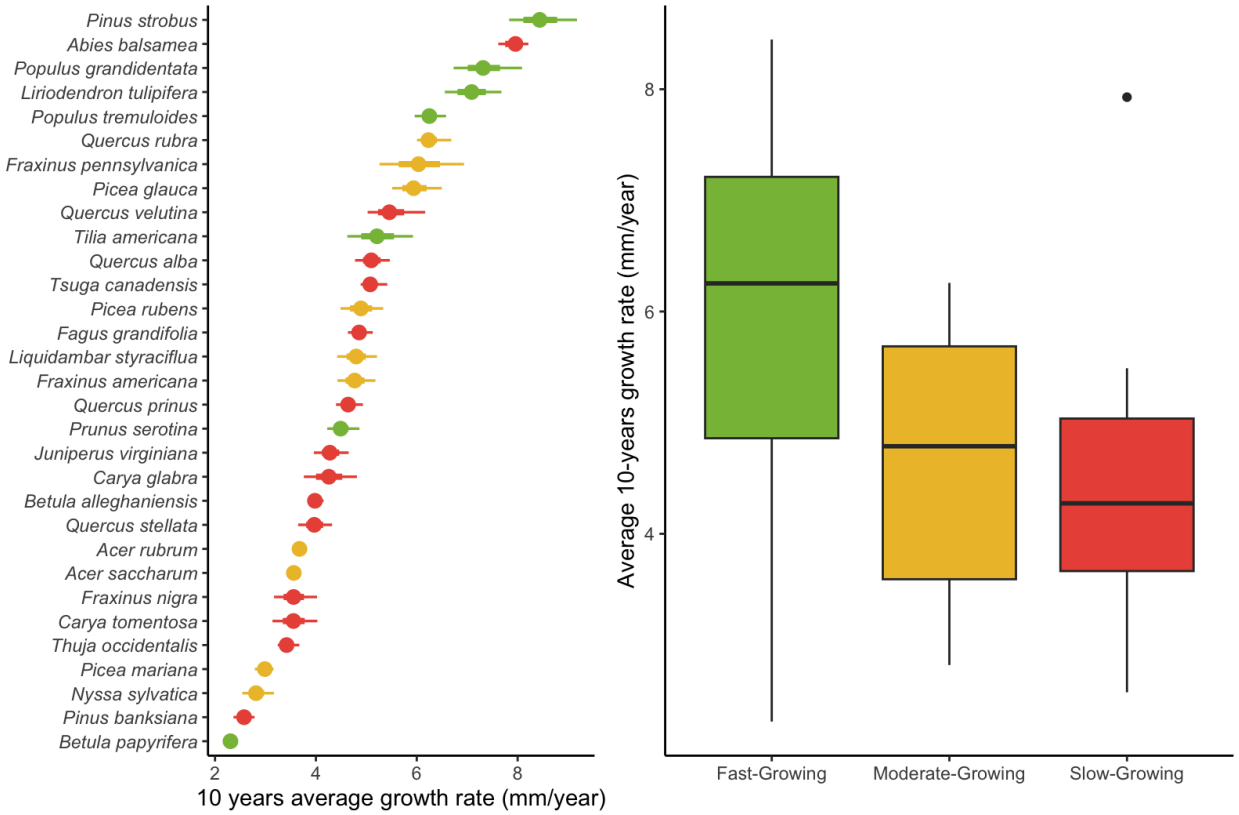


Figure 8: Posterior distribution for the intercept of the growth model using the 10-year average growth rate. Species are classified by their general growth trait following Burns et al. (1990).

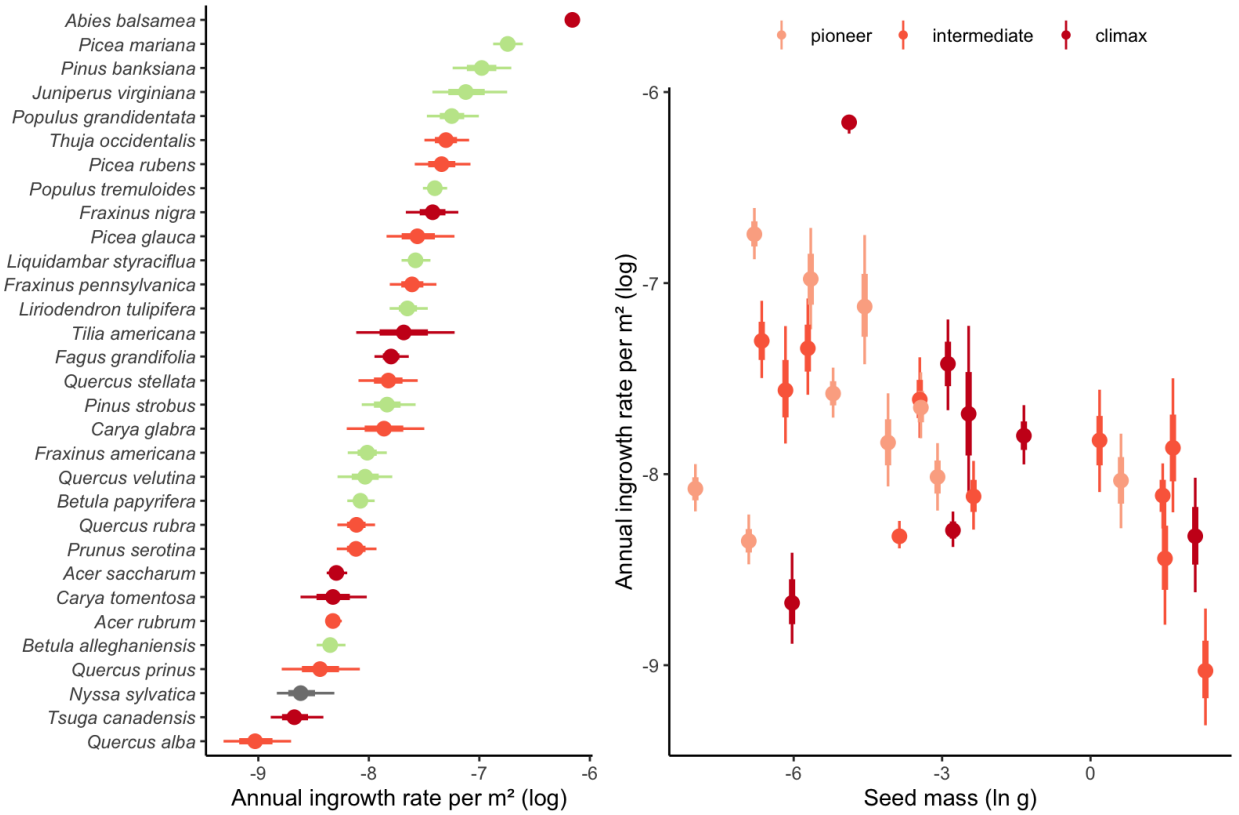


Figure 9: Posterior distribution for the intercept of the ingrowth model for the number of individuals that ingress the population per year per m^2 in function seed mass (Díaz et al. 2022). Species are classified by their successional status following Burns et al. (1990).

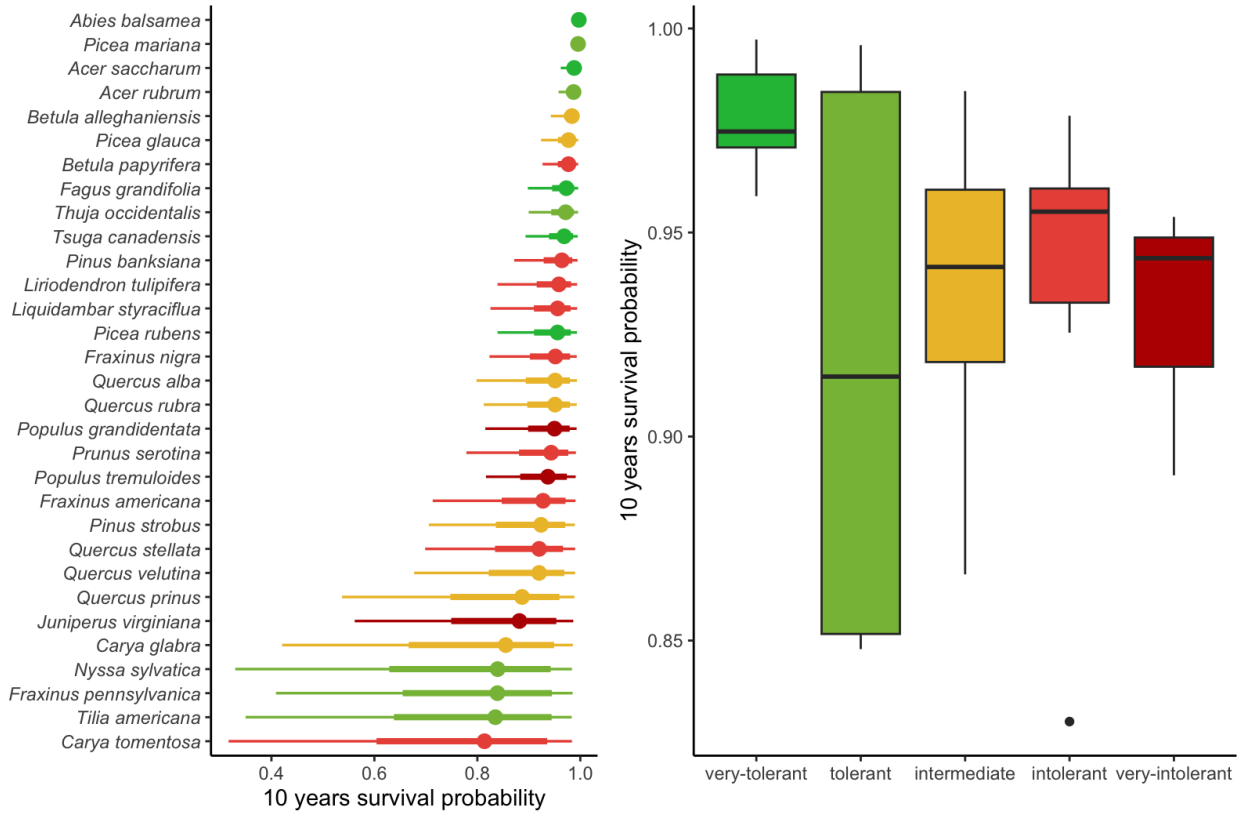


Figure 10: Posterior distribution for the intercept of the annual survival probability for the ingrowth model. Species are classified by their shade tolerance trait following Burns et al. (1990).

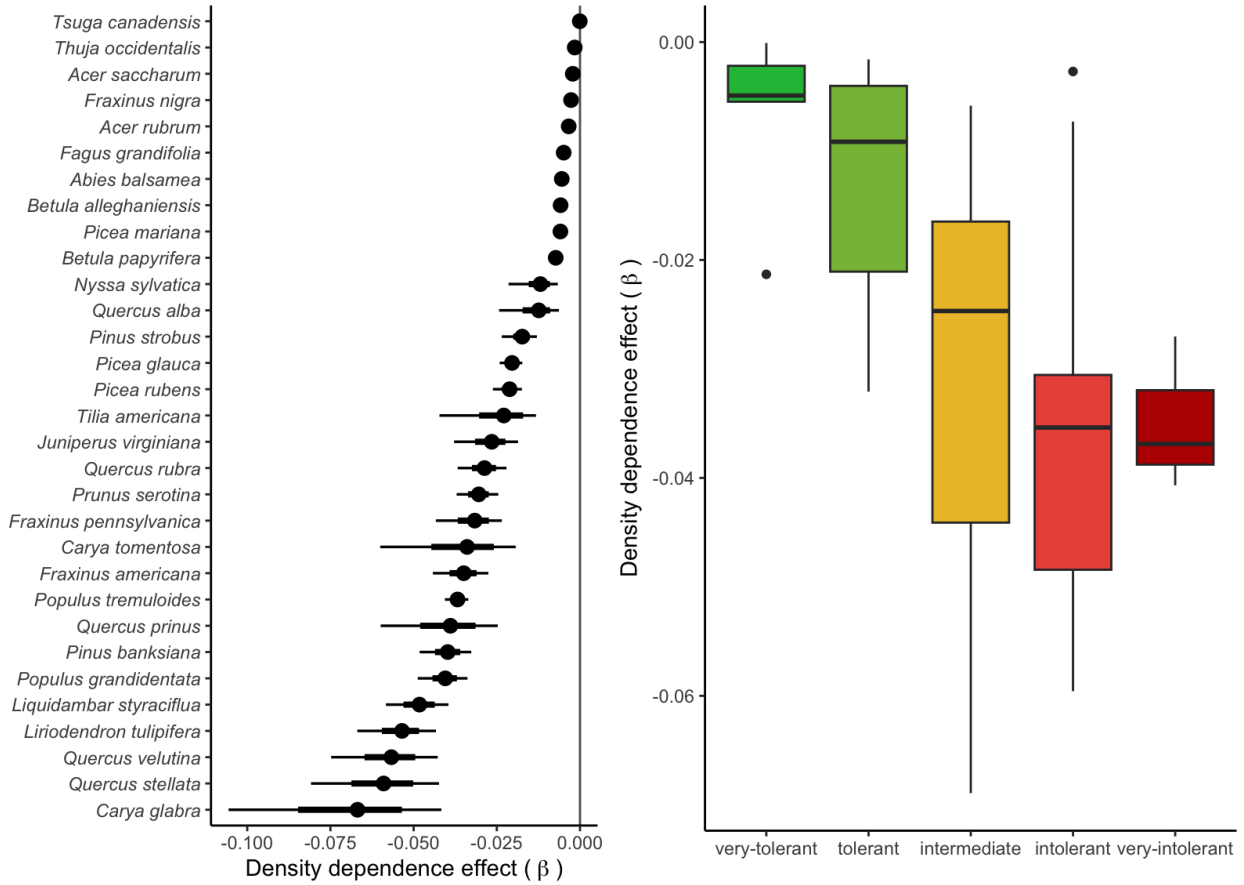


Figure 11: Posterior distribution of the density dependence parameter affecting the annual survival rate of recruitment individuals. Species are classified by their shade tolerance trait following Burns et al. (1990).

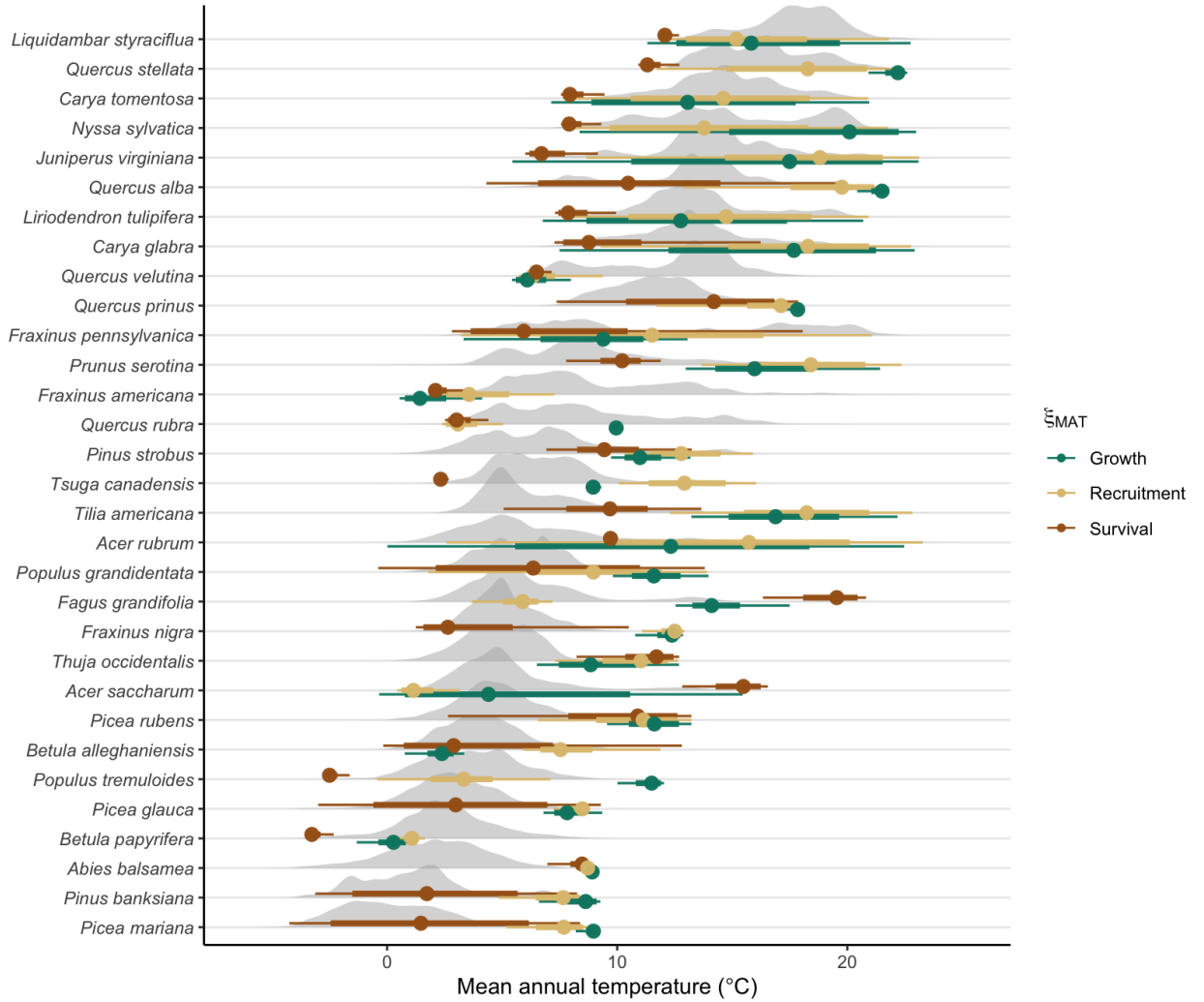


Figure 12: Distribution for the optimal annual mean temperature (ξ_{MAT}) for growth (green), recruitment (yellow), and survival (brown). The gray density plot is the annual mean temperature distribution among all observed trees across space and time.

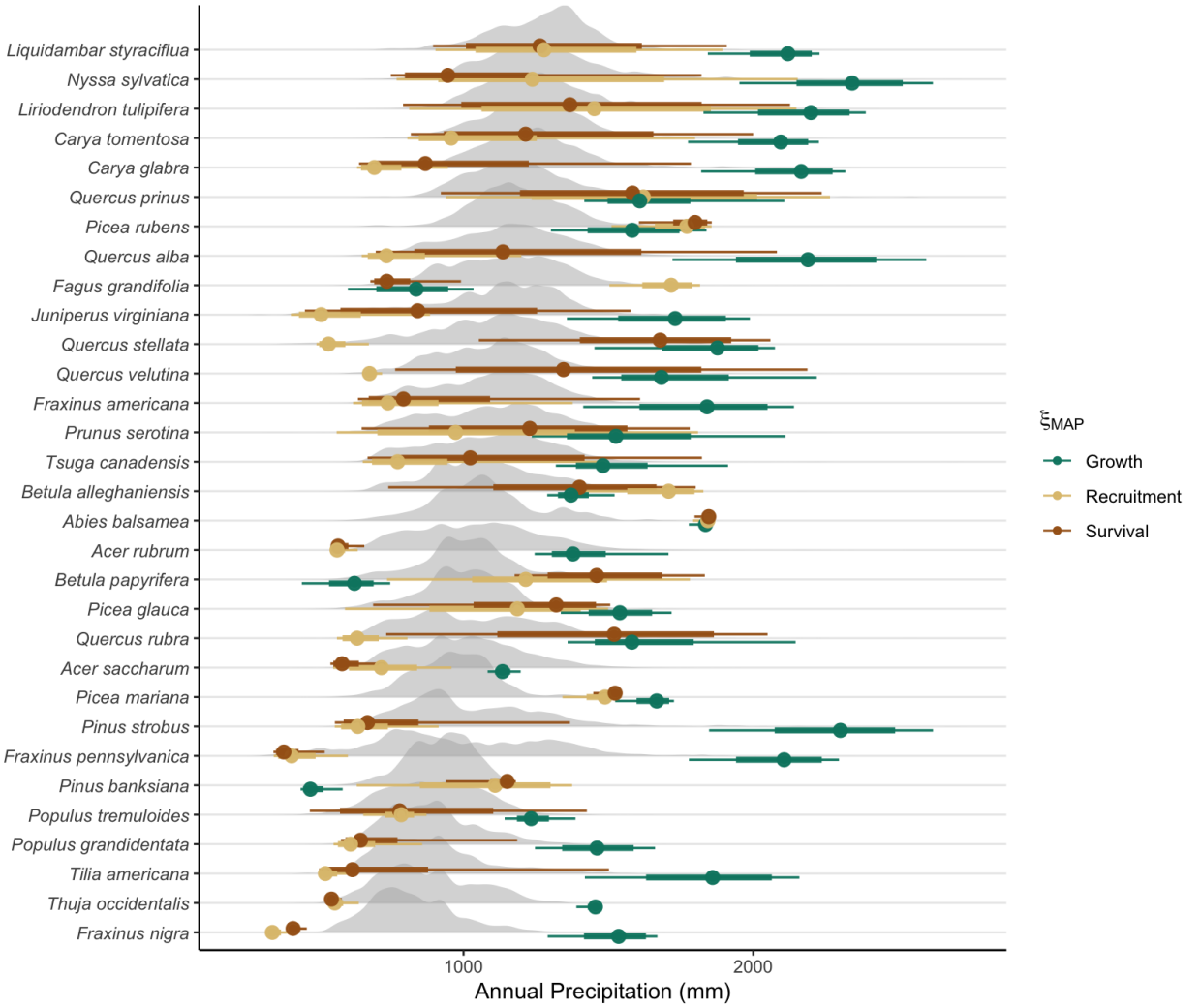


Figure 13: Distribution for the optimal mean annual precipitation (ξ_{MAP}) for growth (green), recruitment (yellow), and survival (brown). The density plot in gray is the distribution of annual precipitation variable among all observed trees across space and time.

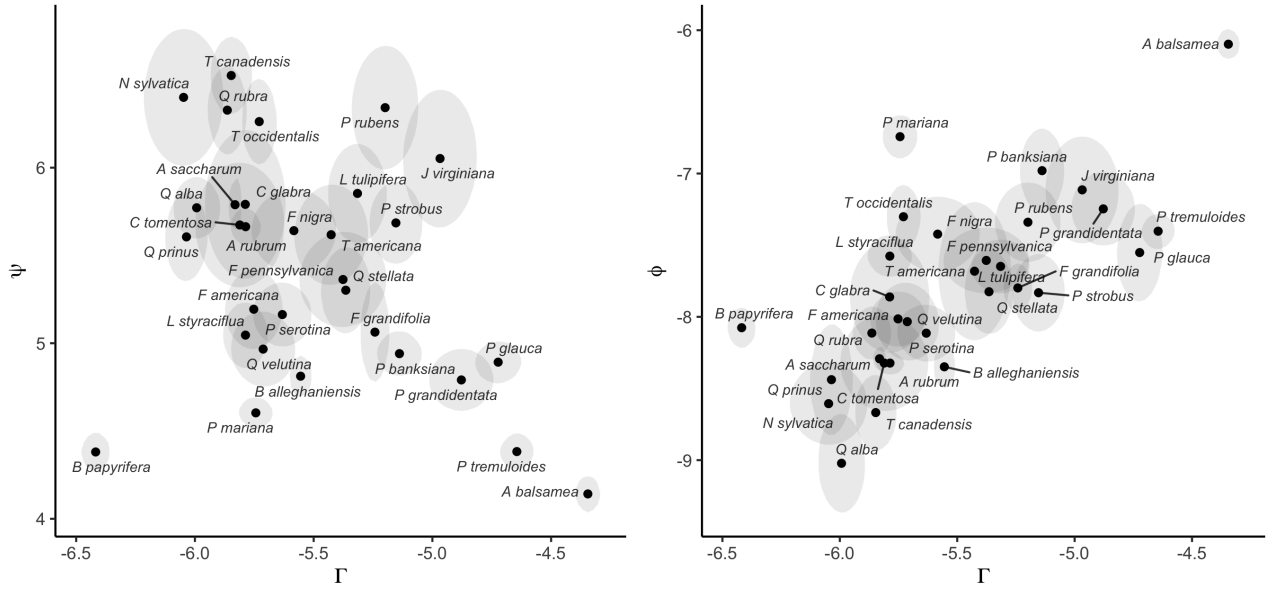


Figure 14: Correlation between (left panel) growth rate (Γ) and annual survival rate (ψ) and (right panel) growth rate (Γ) and annual recruitment rate (ϕ). The uncertainty of the parameters is summarised by a Multivariate Normal Density function with 90% probability.

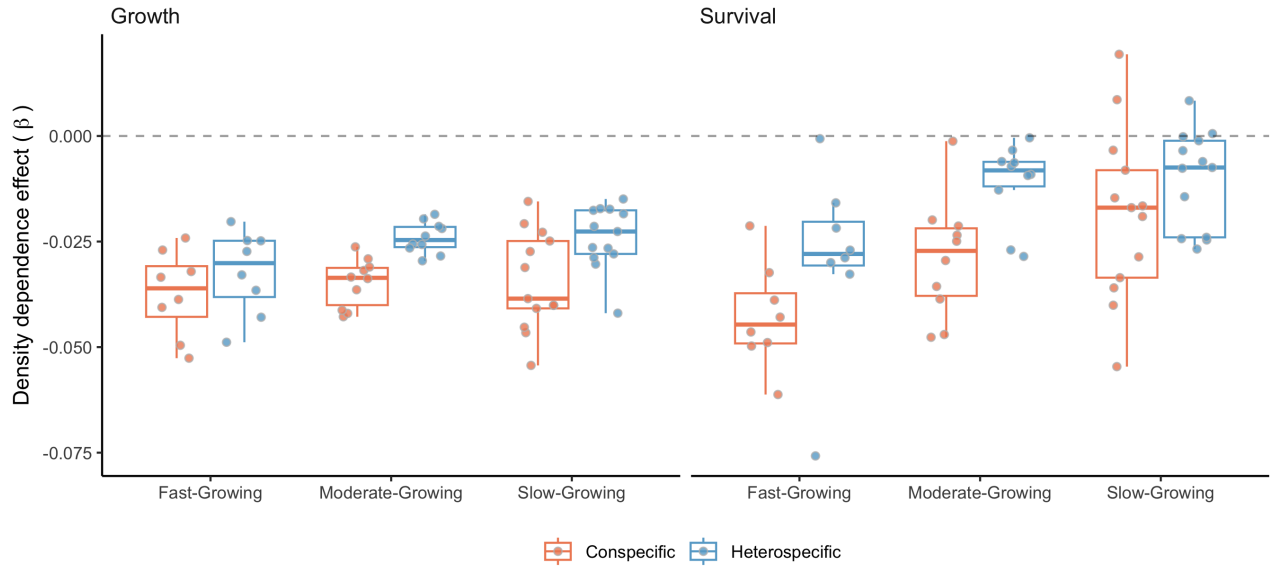


Figure 15: Posterior distribution for the conspecific (red) and heterospecific (blue) density dependence for each class of growth rate (Burns et al. 1990). The more negative the β , the stronger the competition effect.

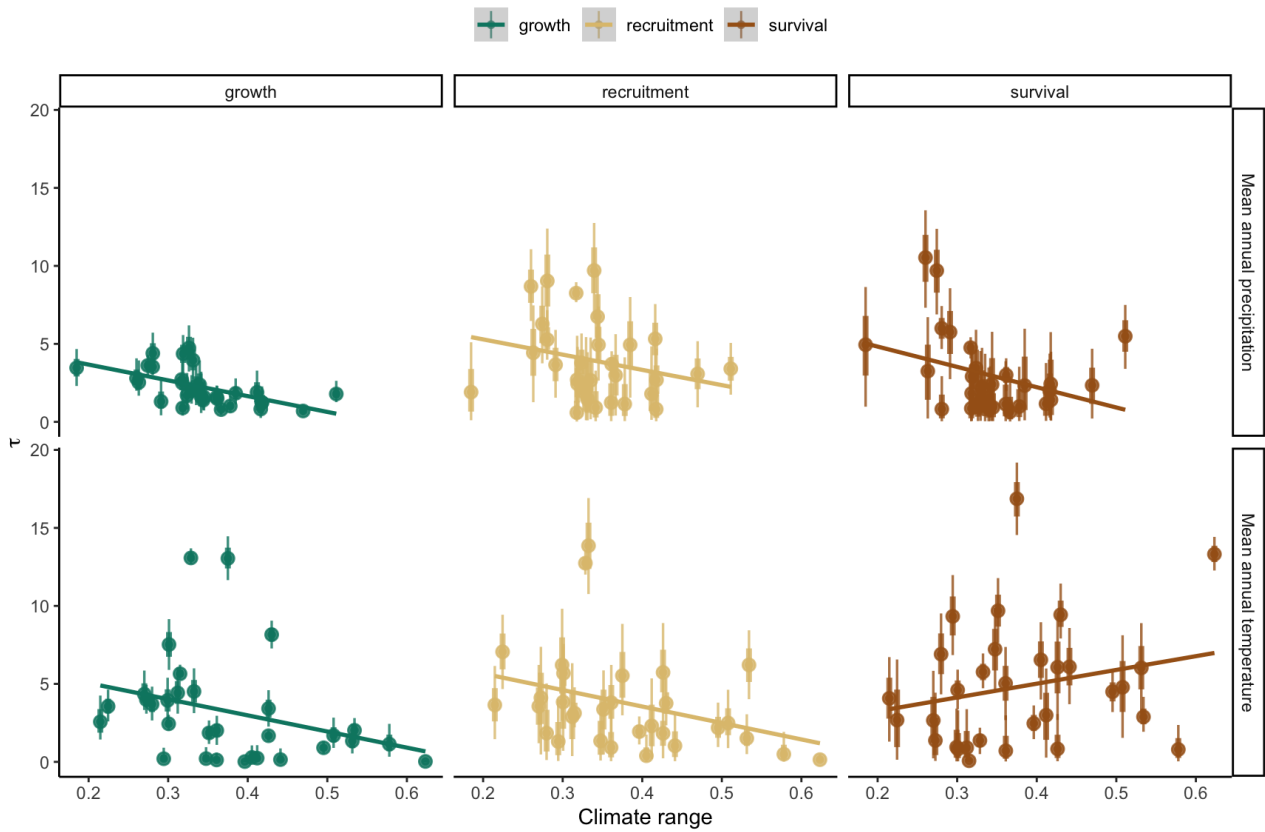


Figure 16: Climate breadth in function of climate range size. The higher the climate range size, the more climate conditions the species experienced.

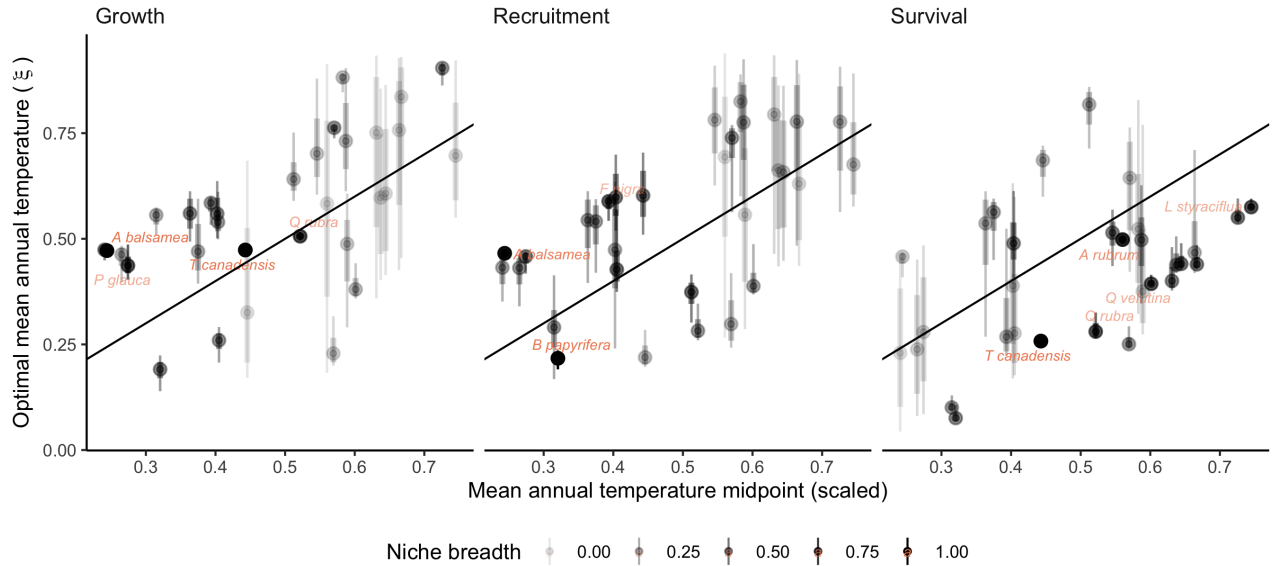


Figure 17: Correlation between posterior distribution of optimal temperature (ξ_{MAT}) and the species' midpoint location across the mean annual temperature range. The transparency of each species point is scaled to be a function of niche breadth. The closer this value is to zero, the higher the breadth around the mean. In other words, when climate breadth is zero, the bell-shaped unimodal function becomes an almost flat line. Colored species names are those with niche breadth higher than 0.5.

96 **3 Supplementary Mateiral 3**

97 **3.1 Sensitivity analysis**

98 Here, we conducted a global sensitivity analysis (GSA) of the population growth rate (λ) with respect
99 to demographic models. Sensitivity analysis uses various methods to decompose the total variance of
100 an outcome into contributions from parameters or input variables. In structured population models,
101 sensitivity analyses involve computing partial derivatives of λ to individual parameters, following
102 Caswell (1978) as:

$$\frac{\partial \lambda}{\partial \theta_i} \quad (1)$$

103 where theta represents a vector of i parameters. However, most methods quantify the local sensitivity
104 of each parameter separately while holding all others constant (Saltelli et al. 2019). This approach can
105 overlook the obscure parameter interactions often common in complex models. Furthermore, because
106 of the high dimensionality of IPM due to the large number of parameters, these methods can quickly
107 become computationally expensive.

108 To address this, we leveraged the efficiency of non-parametric models, such as random forests, for
109 variable importance classification (Antoniadis et al. 2021). This approach offers speed and suits
110 our study as it allows us to quantify both sources of variability in λ . It accounts for the sensitivity
111 of λ to each parameter and considers the uncertainty associated with the parameters. Therefore, a
112 specific parameter may have higher importance because either λ is more sensitive to it or because the
113 parameter is more uncertain.

114 We quantified the variability in population growth rate in function of the parameters using an *insileco*
115 experimental approach. Specifically, we quantified the variability λ for different climate conditions,
116 ranging from cold to the center and up to the hot mean annual temperatures experienced by each
117 species. Furthermore, we combined the climate conditions with a low and high competition intensity.
118 We defined the temperature ranges for each species using the 1st, 50th, and 99th percentiles. The low
119 competition was defined as a population size of $N = 0.1$, while high competition was set at the 99th
120 percentile of the plot basal area. Precipitation was kept at optimal conditions computed based on the

121 average optimal precipitation parameters among growth, survival, and recruitment models.

122 For each species, climate, and competition conditions, we computed λ 500 times using different draws
123 from the posterior distribution, setting the plot random effects to zero. The code used for this analysis
124 can be found in the [forest-IPM](#) GitHub repository.

125 3.2 Simulation Summary

126 The final simulation involved a total of 500 draws across species and different conditions. The Figure
127 18 illustrates the distribution of λ computed using 500 random draws from the posterior distribution
128 of parameters across different climate and competition conditions.

129 3.3 Importance of demographic models

130 Random forest is a non-parametric classification or regression model that ranks each input variable's
131 importance in explaining the variance of the response variable. We used the permutation method for
132 ranking variable importance (Breiman 2001). This method measures the change in model performance
133 by individually shuffling (permuting) the values of each input variable. The greater the change in
134 predictive accuracy with shuffling input values, the more important the specific variable will become.
135 This is computed individually for each tree and then averaged across all n random trees. Finally,
136 we normalized the importance output of each regression model so that they sum to 1. We used the
137 R package `ranger` with default hyperparameters for fitting the random forest models (Wright and
138 Ziegler 2017).

139 Figure 19 shows the distribution of R^2 from 20 random forest replications across different climate and
140 competition conditions. These values range from 0.2 to 0.9, with an average value of 0.63 across species
141 and conditions. This variation possibly reflects the uncertainty in the parameters across species.

142 As our primary interest lies in demographic levels rather than parameter levels, we focus on the
143 combined importance of all parameters for each demographic model. This splits the total importance
144 among the four demographic functions of the IPM: growth, survival, recruitment, and recruited size
145 models. The recruited size model had an insignificant contribution to λ , with nearly all random forest
146 models showing a contribution below 1%. Thus, we omitted this model and concentrated on the
147 growth, survival, and recruitment models, which collectively explain over 99% of the variation in λ

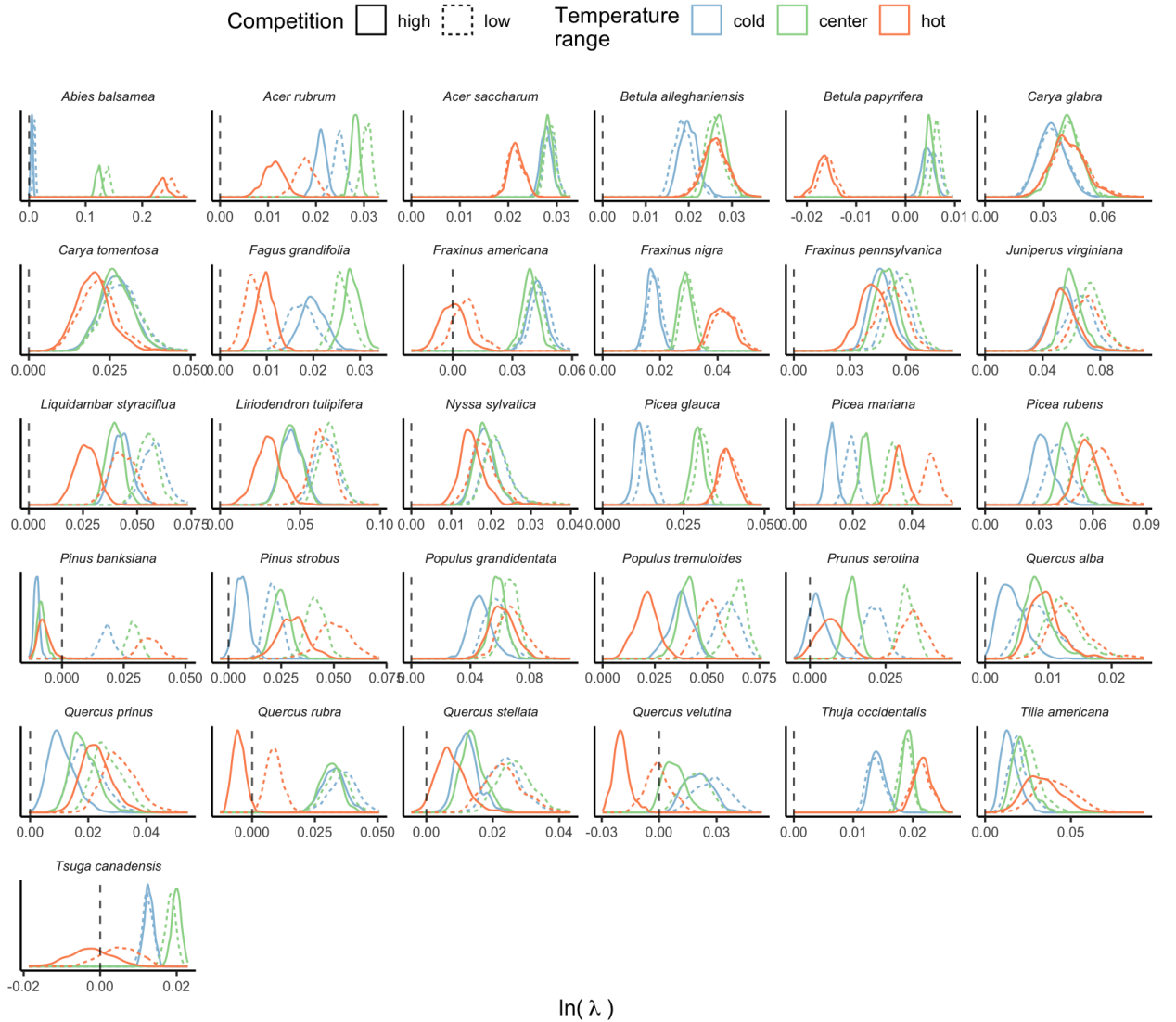


Figure 18: Distribution of 500 draws of population growth rate (λ) for different climate and competition conditions

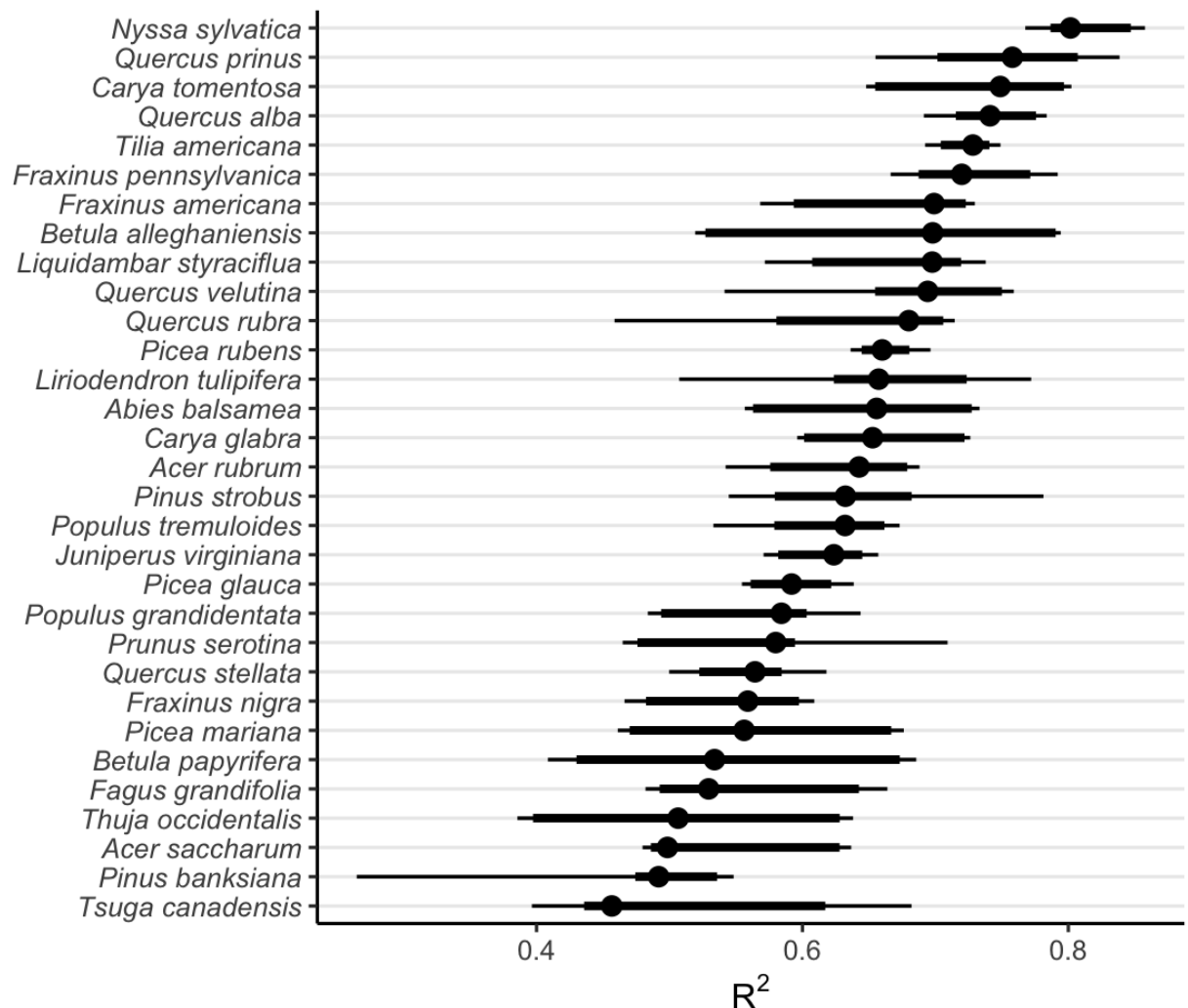


Figure 19: Distribution of R^2 from 20 random forest replications across different climate and competition conditions.

148 (Figure 20).

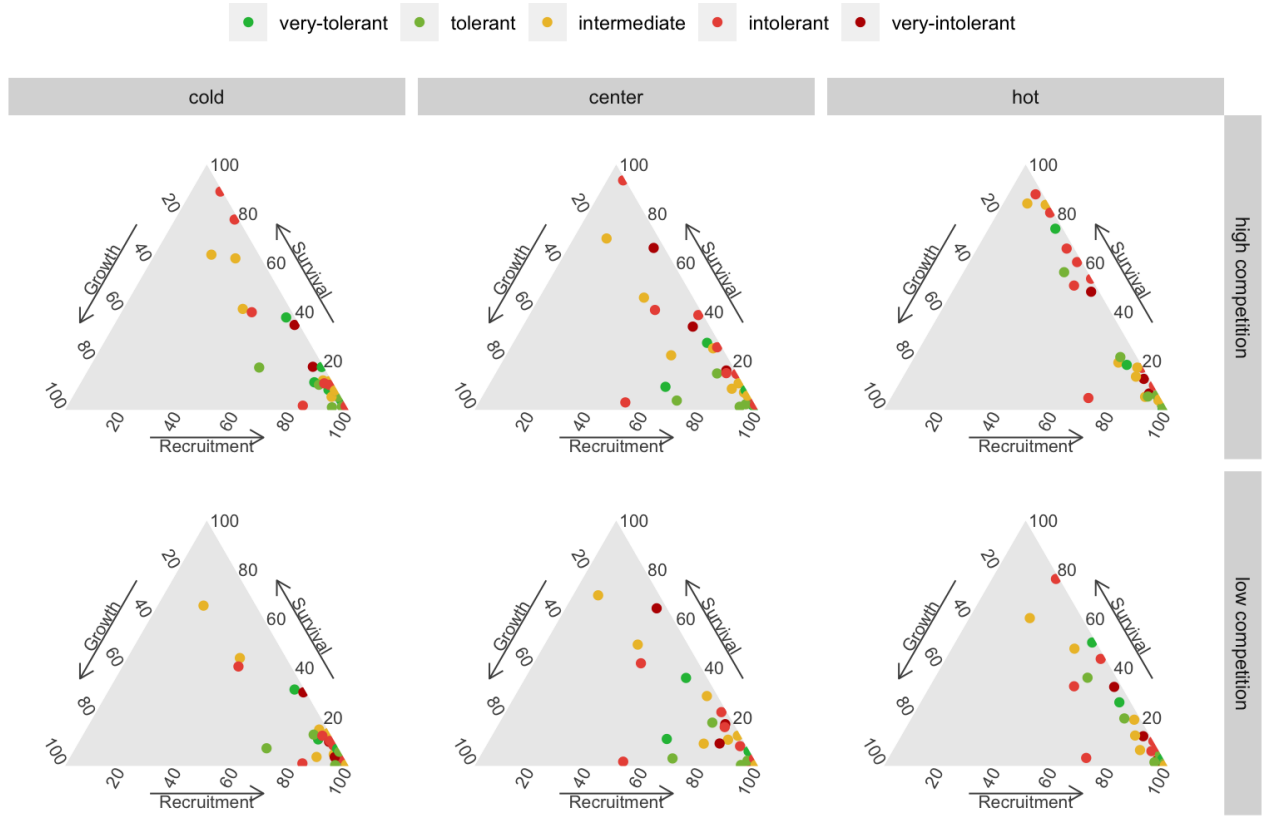


Figure 20: Ternary plot describing the importance distribution among the growth, survival, and recruitment models. Color represents the level of shade tolerance (Burns et al. 1990).

149 The ternary plots above show the raw importance data from the random forest, which can be challenging
150 to interpret. The key message is that variance in λ is primarily explained by the recruitment and
151 survival demographic models. Furthermore, certain conditions appear to shift the importance from
152 recruitment to the survival model. In Figure 21, we explore the correlation between the importance of
153 recruitment and survival under different covariate conditions.

154 We observe that at low competition, for most species, variations in λ are primarily explained by
155 recruitment. This pattern slightly diminishes as we move from the cold range to the center and up
156 to the hot temperature range. We can observe an overall shift toward the survival model at high
157 competition intensity, especially in the hot temperature range.

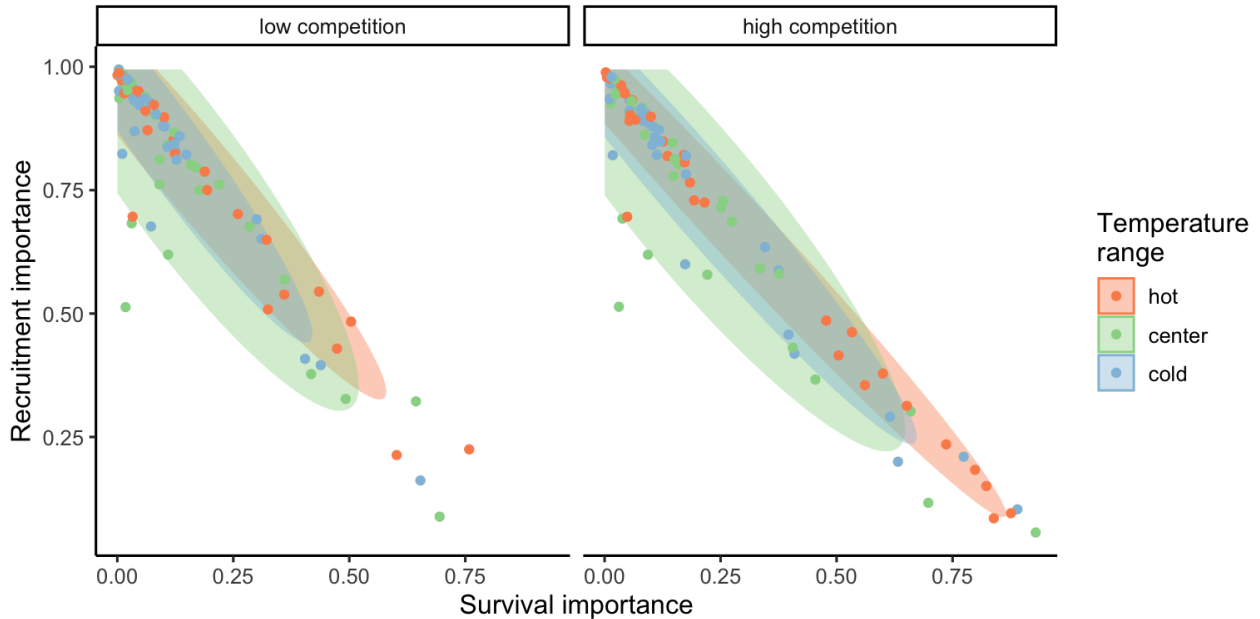


Figure 21: Correlation between the survival and recruitment relative importance across the 31 species, climate and competition conditions. Species points are grouped by a Multivariate Normal Density function with a probability of 90%.

158 3.4 Importance of covariates

159 Similar to assessing parameter importance, we also used the random forest approach to evaluate the
 160 importance of covariates. For simplicity, we used the same output of the simulations as previously
 161 explained, shifting the explanatory variables from parameters to covariates.¹ The Figure 22 shows the
 162 distribution of relative importance between climate and competition covariates for each species.

163 3.5 Notes on Conspecific and Heterospecific Competition Effects

164 In the preceding discussion, we did not specify whether we were considering conspecific or heterospecific
 165 competition. For all the results presented in this chapter, the *high competition* condition was applied
 166 at the heterospecific level, while conspecific competition was set to a very low proportion. This choice
 167 is based on the standard invasion growth rate metric, or the population growth rate when rare, an
 168 important measure for quantifying population persistence (Lewontin and Cohen 1969).

169 Additionally, we performed the sensitivity analysis with the same conditions, except for changing
 170 the high competition from heterospecific to conspecific individuals. We observed that nearly all the

¹This analysis could be expanded to include more marginal conditions beyond just cold, center, and hot temperatures and low and high competition. However, this would exponentially increase the number of simulations.

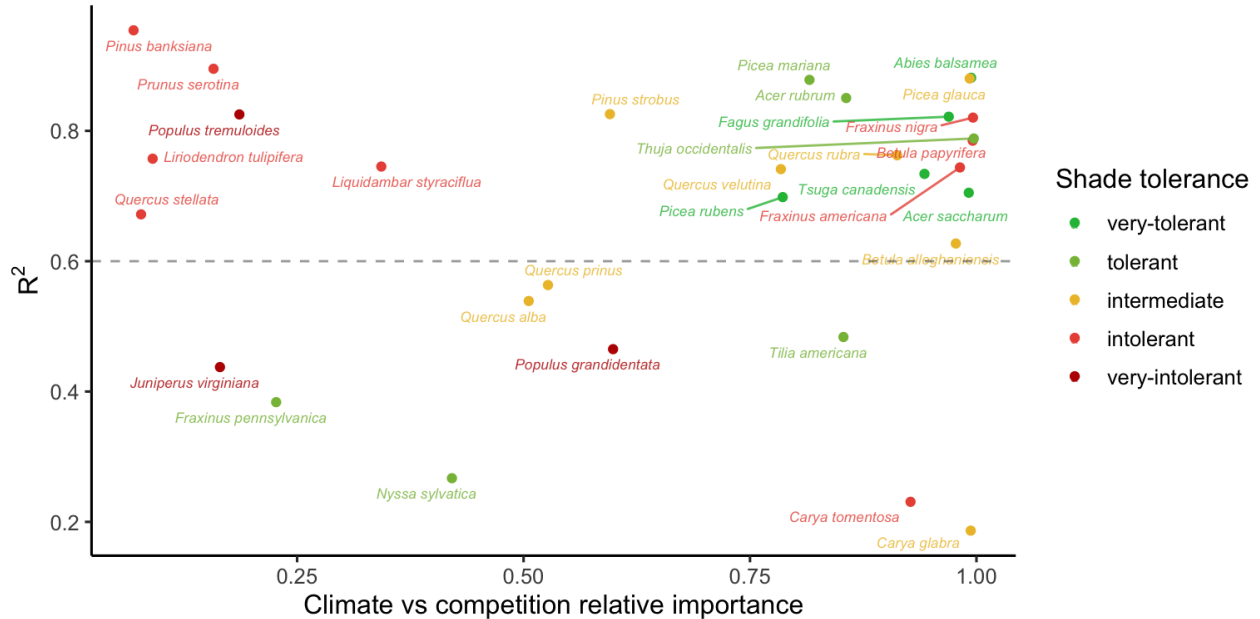


Figure 22: Distribution of relative importance between climate and competition covariates according to Random Forest, the respective R^2 . The more species are to the right of the panel, the more climate is important relative to competition. Color represents the level of shade tolerance (Burns et al. 1990)

171 variation in λ , previously attributed to the growth model, shifted to the recruitment model. Also, the
 172 importance attributed to the survival model for certain species at the center and cold temperature
 173 conditions shifted toward the recruitment model. Although we observed this shift, the overall patterns
 174 remained similar to those discussed earlier. The only exception was the distribution of relative
 175 importance between climate and competition (Figure 22), where many species had an increase in the
 176 importance of competition relative to climate. These observed differences primarily arise from the
 177 high sensitivity of λ to the ϕ parameter.

178 References

- 179 Antoniadis, A., S. Lambert-Lacroix, and J.-M. Poggi. 2021. Random forests for global sensitivity
 180 analysis: A selective review. Reliability Engineering & System Safety 206:107312.
- 181 Breiman, L. 2001. Random forests. Machine learning 45:5–32.
- 182 Burns, R. M., B. H. Honkala, and Others. 1990. Silvics of North America: 1. Conifers; 2. Hardwoods
 183 Agriculture Handbook 654. US Department of Agriculture, Forest Service, Washington, DC.

- 184 Caswell, H. 1978. A general formula for the sensitivity of population growth rate to changes in life
185 history parameters. *Theoretical population biology* 14:215–230.
- 186 Díaz, S., J. Kattge, J. H. C. Cornelissen, I. J. Wright, S. Lavorel, S. Dray, B. Reu, M. Kleyer, C. Wirth,
187 I. C. Prentice, and Others. 2022. The global spectrum of plant form and function: enhanced
188 species-level trait dataset. *Scientific Data* 9:755.
- 189 Gabry, J., R. Češnovar, and A. Johnson. 2023. cmdstanr: R Interface to 'CmdStan'
190 Lewontin, R. C., and D. Cohen. 1969. On population growth in a randomly varying environment.
191 Proceedings of the National Academy of sciences 62:1056–1060.
- 192 Saltelli, A., K. Aleksankina, W. Becker, P. Fennell, F. Ferretti, N. Holst, S. Li, and Q. Wu. 2019.
193 Why so many published sensitivity analyses are false: A systematic review of sensitivity analysis
194 practices. *Environmental modelling & software* 114:29–39.
- 195 Team, S. D., and Others. 2022. Stan modeling language users guide and reference manual, version
196 2.30.1. Stan Development Team.
- 197 Vehtari, A., A. Gelman, and J. Gabry. 2017. Practical Bayesian model evaluation using leave-one-out
198 cross-validation and WAIC. *Statistics and computing* 27:1413–1432.
- 199 Wright, M. N., and A. Ziegler. 2017. {ranger}: A Fast Implementation of Random Forests for High
200 Dimensional Data in {C++} and {R}. *Journal of Statistical Software* 77:1–17.